1

Computational Study of Solvent Incorporation into a Porphyrin Monolayer.

K. W. Hipps \* and Ursula Mazur Department of Chemistry Washington State University

Pullman, WA 99164-4630

\*Email: hipps@wsu.edu

**ABSTRACT** 

Density functional theory (DFT) is used to investigate the conversion from a solvent incorporated pseudo-polymorph into a single component monolayer. Calculations of thermodynamic properties both for the surfaces in contact with gas phase and with solvent are reported. In the case of wetted surfaces, a simple bond-additivity model, first proposed by Campbell and modified here, is used to augment the DFT calculations. The model predicts a dramatic reduction in desorption energies in solvent as compared to gas phase. Eyring's reaction rate theory is used to predict limiting desorption rates for guest (solvent) molecules from the pockets in the pseudo-polymorph and for cobalt octaethylporphyrin (COEP) molecules in all structures. The pseudo-polymorph studied here is a nearly rectangular lattice (REC) composed of two CoOEP and 2 molecules of either 1,2,4-trichlorobenzene (TCB) or toluene (TOL) supported on 63 atoms of Au(111). At sufficiently high initial concentrations of CoOEP, only a hexagonal unit cell (HEX) with two molecules of CoOEP, supported on 50 atoms of gold is observed. Experimentally, the TCB-REC structure is more stable than the TOL-REC structure existing in solution at initial mM concentrations of CoOEP in TCB as opposed to initial µM concentration of CoOEP in toluene. Calculations here show that the HEX structure is the thermodynamically stable structure at all practical concentrations of CoOEP. Once the REC structure forms kinetically at

low concentration because of the vast excess of solvent on the surface, it is difficult to convert to

the more stable HEX structure. The difference in stability is primarily due to the difference in electronic adsorption energy of the solvents (TOL or TCB) and to the very low desorption rate of CoOEP. The adsorption energy of TCB has two important contributors: the adsorption energy onto Au alone, and the intermolecular interactions between TCB and the CoOEP host lattice. Neither factor can be neglected. We also find that planar adsorption of both TOL and TCB on Au(111) is the energetically preferred orientation when space is available on the surface.

Rates of desorption are very sensitive to the solvent free activation energy and to the thermodynamic parameters required to convert the solvent free activation energy to one for the solvated surface. Small changes in the computed energy (of the order of 5%) can lead to one order of magnitude change in rates. Further, the solvation model used does not provide the barrier to adsorption in solution needed to determine values for the desorption activation energy. Thus, the rates computed here for desorption into solvent are limiting values.

# INTRODUCTION

Density functional theory (DFT) has been used extensively in the study of molecular and crystalline porphyrin systems.<sup>1-7</sup> DFT has also been used to study porphyrins and other large conjugated systems on surfaces. <sup>8-15</sup> True polymorphism has also been the subject of study by DFT methods. <sup>16-21</sup> Much less studied by DFT are systems with two components (tectons) making up the self-assembled monolayer. Examples include the porphyrin-coronene system, <sup>22</sup> guest-host systems like the PBM2-coronene system, <sup>23</sup> and the incorporation of Zn and Ag nitrates into pores created by trimesic acid cycles on graphite. <sup>24</sup> Of particular interest in relation to the present work is the near absence of papers using DFT to study solvent molecule incorporation into a non-covalent SAM.

Recently, Gurdumov and coworkers published experimental studies of the effects of solvent on the structure and kinetics of cobalt octaethylporphyrin (CoOEP) self-assembled monolayers (SAMS) on HOPG<sup>25</sup> and on Au(111)<sup>26</sup>. They found that on HOPG, a CoOEP pseudo-hexagonal (HEX) structure containing two CoOEP per unit cell was formed from toluene (TOL), phenyloctane (PhO) and decane (DEC) solution. The term pseudo-polymorph indicates a structural variation resulting from incorporation of another species (usually solvent) into a structure. <sup>27</sup> When 1,2,4-trichlorobenzene (TCB) is used as solvent for the tecton (CoOEP), TCB is incorporated into the SAM forming a nearly rectangular (REC) lattice having one CoOEP and one TCB per unit cell. On Au(111), however, both toluene and TCB (at low initial concentrations of CoOEP) form REC structures, but these contain two CoOEP and two solvent molecules per cell. The toluene REC structure was unstable and converted to HEX (with elimination of toluene) with time except at the very lowest concentrations of CoOEP studied (≤ 1 μM). The TCB REC structure was much more durable. The authors provided some preliminary structural DFT

calculations for the HOPG structures, and contrasted the adsorption energies of the TOL and TCB on HOPG and Au.

Considering that TOL and TCB are of similar size and both have similar  $\pi$  structure, why would one be significantly more stable than the other? This is an important fundamental question that goes well beyond this particular system. Thus, a more detailed computational exploration of this interesting pseudo-polymorph system is justified. While the data presented by Gurdumov is for the solution-solid interface, we will consider both the vapor-solid and solution-solid interfaces. This study captures a number of interesting features associated with pseudo-polymorph formation and with adsorption into cavities formed by molecules that are not entirely planar. Included in our calculations are the vibrational frequencies of all the modes of the TOL and TCB within the REC structure, as well as those for the gas phase. Barriers to rotation in the REC structure and to desorption are calculated. The desorption potential energy curves for TOL and TCB in REC, and for the same molecules at low coverage on Au(111) are also computed and provide insights into factors relating to energies of solvent incorporation. Rates of desorption of solvent into the vapor from the pockets formed in the REC structure, and for CoOEP, are computed. The DFT calculations are performed for the surface in contact with the vapor. Using a model first proposed by Campbell <sup>28,29</sup>, and modified here, we are able to calculate desorption energies and equilibrium concentrations as well as limiting values for the rates of molecular desorption from the surface in contact with solvent.

## **METHODS**

Computations are performed with density functional theory (DFT) using the Vienna Ab-initio Simulation Package (VASP)<sup>30,31</sup> version 6.2.0 or with the program Gaussian 16.<sup>32</sup> Some of the CoOEP free molecule DFT calculations were performed using the UB3LYP-gd3 functional and

the 6-311G++(d,p) basis. The VASP code uses the projector augmented wave (PAW) method<sup>33,34</sup> to describe the core electrons and valence-core interactions. We used both the optB88-vdW functional<sup>35,36</sup> and the meta-GGA SCAN+rVV10 functional,<sup>37</sup> with PAW potentials optimized for the PBE functional<sup>38</sup> for all calculations. The electronic wavefunctions were determined at the Gamma ( $\Gamma$ ) point in the irreducible Brillouin zone. A plane wave cut off energy of 500 eV was used for all simulations. For the Au(111) and adsorbate-Au(111) systems, Methfessel-Paxton smearing was used to set the partial occupancies for each wave function with a smearing width of 0.2 eV. For the isolated molecular systems Gaussian smearing was used with a width of 0.04 eV. All the geometries were fully optimized to less than 0.5 meV energy convergence and less than 0.02 eV/A forces. The choice of our DFT methodology, plane wave cutoff energies and k-point choice were based on previous periodic DFT simulations of similar systems of type<sup>7,8,22,39-41</sup> and size. 42 VASP calculations were performed on species adsorbed to 3-layer unreconstructed Au and on the same species in the gas phase. During optimizations, only the top layer of Au was allowed to vary in position. The REC and HEX cell dimensions were chosen to match the unit cell dimensions given by Gurdumov for the REC and HEX cells. <sup>26</sup>  $\mathbf{a_r} = 10\mathbf{a_1} + 11\mathbf{a_2}$ ,  $\mathbf{b_r} = -3\mathbf{a_1} + 3\mathbf{a_2}$ , and  $\mathbf{a_h} = \mathbf{a_r}$  with  $\mathbf{b_h} = 5\mathbf{a_2}$ , for the REC and HEX cells, respectively. Where  $\mathbf{a_1}$  and  $\mathbf{a_2}$  are the Au(111) atomic lattice vectors and are separated by 120°. Cells had at least 1.8 nm vacuum space above the highest point on the monolayer surface.

It should be noted that these are huge cells having significantly more than 300 atoms. The HEX cell has 320 atoms while the REC cells have more than 380. They required significant computational time even with the assumptions of some of the atoms being fixed. The calculations reported here are relatively basic periodic DFT calculations, with the only exception being the more sophisticated optB88-vdW or SCAN+rVV10 functionals. One can rightly ask how these

results might change if we used more k points or more layers of Au as substrate. In order to get some insight into this, while still completing the work in a finite time, we did two test computations. First, we computed the desorption energy of one TCB from the TCB-REC unit cell using (1, 2, 1) as the number of k points (doubling the number). We found that the desorption energy changed by less than 1%. This is likely due to the very large supercells used. Second, we considered the desorption energy of TCB (only) from gold both with a 3 layer and 5 layer gold. The difference here with the thicker Au substrate was less than 20 meV. Thus, we are confident that these calculations reflect the actual nature of the problem within the constraints imposed by the computational method and the functional chosen. CONTCAR files for the optimized CoOEP-TCB-REC and CoOEP-HEX systems are provided in the supplemental materials. Adsorption energies were calculated as the energy of the optimized adlayer on gold minus the energy of the optimized gold minus the energy of the isolated optimized molecules.

Calculations were performed to determine vibrational frequencies of TCB and TOL in the REC lattice and also as free molecules. The same B88vdW functional was used as for the structure optimizations but Hessian calculations with finite differences (a step size of 0.015 Angstroms, and two symmetrical steps per degree of freedom) were used. Because of the complexity of the unit cell, all atoms except those of TCB or TOL were fixed at their previously optimized positions during the evaluation of vibrational frequencies for TCB and TOL.

Many single point calculations were done in order to determine barrier heights for motions such as the frustrated translations and rotations. We also calculated the adsorption potential energy surfaces for adsorption into the REC lattice and onto Au(111) at low TCB or TOL coverage (about 0.2 monolayer). In the REC adsorption case, we used nudged elastic band methods<sup>43</sup> with the B88vdW functional to find a more precise value of the barrier to escape of the TCB (parallel

orientation) from the CoOEP pocket. In the TCB-REC case we computed the desorption electronic energy curve with the SCAN+rVV10 functional for the parallel orientation allowing the monolayer to relax to its minimum energy/force configuration. We also considered adsorption with the TCB and TOL rings standing up from the surface. In the case of the TCB up configuration, we also computed the adsorption potential curve.

Statistical mechanics and Eyring's absolute reaction rate theory<sup>44</sup> were used to estimate desorption rates for TOL, TCB, and CoOEP. In order to estimate the energy of the transition state in the presence of solvent, we used a slightly modified version of the bond additivity model proposed by Campbell.<sup>28, 29</sup> The primary modification is to include the entropic contribution to the surface energy (as opposed to free energy),  $-T(d\gamma/dT)$ , in the calculation of the effect of the solvent on the transition state energy. Details of the method are included in the SI Power Point.

## RESULTS AND DISCUSION

Adlayer Structure: The STM image of the TCB-CoOEP pseudo-rectangular (REC) polymorph on Au(111) as obtained by Gurdumov et al.<sup>26</sup> is shown in Figure 1. Also shown in Figure 1 are the DFT optimized lowest energy structures found for both the persistent TCB pseudo-polymorph and for the TOL pseudo-polymorph. Note that for clarity of viewing, only the top Au layer is shown, but the calculation utilized three Au layers. In order to arrive at these structures, we tried several different starting geometries consistent with the experimental structure. Several were found for the case of the phenyl ring parallel to the gold, but the ones shown were the lowest by at least 2 kcal/mole.

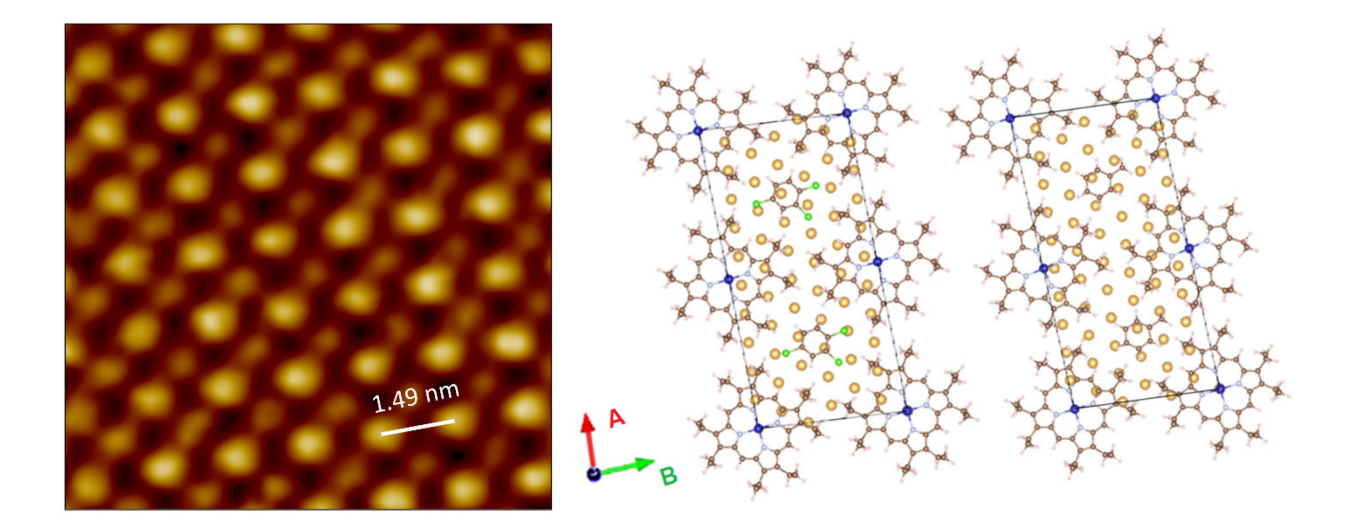


**Figure 1:** STM image of the REC pseudo-polymorph of TCB and CoOEP on Au(111). Also shown are the DFT optimized lowest energy structures found for both the persistent TCB-CoOEP system and the transient TOL-CoOEP pseudo-polymorph. Both structures have a total of 189 Au atoms, with 63 on the surface of the unit cell.

A few previous studies in which TCB appeared as a partner in a pseudo-polymorph suggested that TCB adsorbed edge on (vertical) to gold. <sup>45,46</sup> Thus, it was necessary to consider both parallel and perpendicular geometries for TCB adsorption. We first computed the adsorption energies from the gas phase for TCB alone on Au(111) both parallel to the surface and perpendicular. As shown if **Figure S1**, the surface adsorption potential is remarkably flat for the parallel adsorption of TCB on Au(111) with a maximum variation of about 50 meV. The most stable configuration found had a desorption energy of 1.055 eV. For completeness, we also determined the desorption energy to the gas phase for parallel toluene on Au(111) as shown in **Figure S2**. The most stable configuration for TOL adsorbed from the gas phase parallel to Au(111) has a desorption energy of 0.856 eV. TCB adsorbed vertically is a very different story. The orientation and position of adsorption produces changes greater than 50% in the adsorption energy, and the highest desorption energy (most stable) orientation found was H and 2 Cl's pointed down with each over a Au atom

(**Figure S3**). The energy of this configuration is -0.510 eV, about 12 kcal/mole less stable than any of the parallel adsorption configurations. Thus, for TCB and TOL alone on Au, the flat configuration is most stable.

In the case of the pseudo-polymorph, the interactions of the TCB or TOL with the adjacent CoOEP might make a difference in which configuration is most stable. Thus, we also calculated using the B88vdWW functional the energy of the REC cell where the TCB and TOL molecules are optimized vertically. We began with the TCB in its most stable vertical orientation, with one H and 2 adjacent Cl's down. The result is shown in Figure 2.

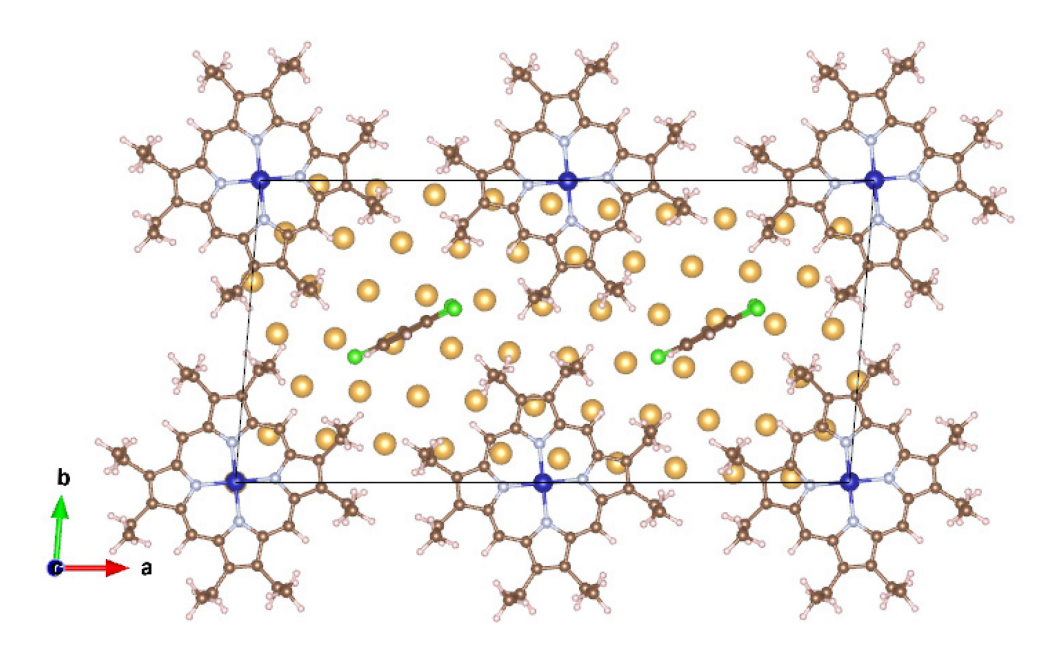
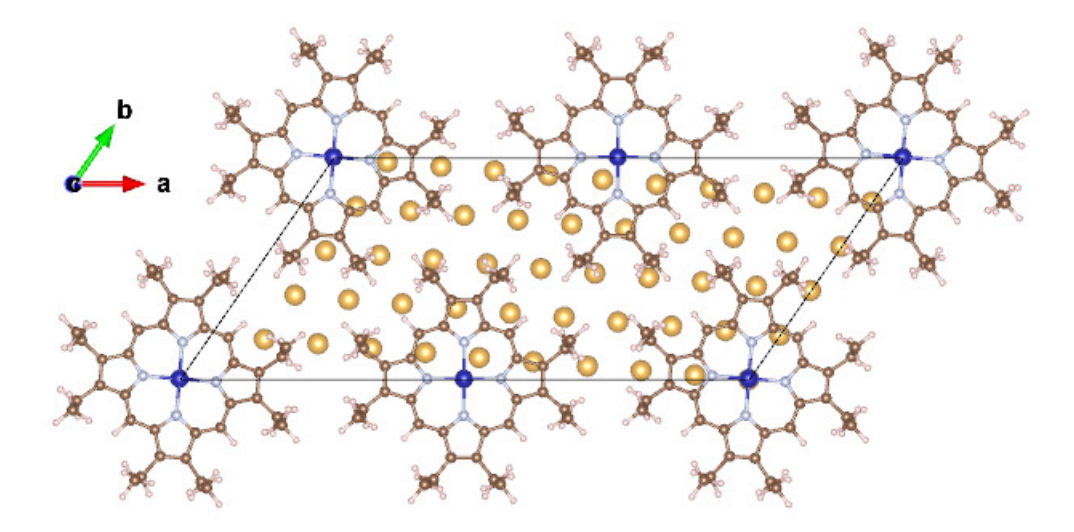


Figure 2: DFT optimized lowest energy structure found for the hypothetical TCB-CoOEP system (in contact with vapor) where the TCB adsorbs vertically to Au(111). The energy of this system is 0.85 eV greater than for the case of parallel adsorption. As in Figure 1, the bottom two layers of Au used in the calculation have been omitted for clarity. The areas of the cells with TCB parallel and perpendicular are identically the same so that the energy difference per unit area is simply 0.85 eV/4.54 nm² (the area of the unit cell). B88vdW functional results.

The calculated electronic energy of the TCB vertical configuration is about 20 kcal/mole greater than that of the parallel configuration (2 TCB up per cell). Thus, we are confident that the REC structure is composed of all flat laying molecules. We also considered the CH<sub>3</sub> down configuration of TOL in the REC structure. For the lowest energy position we found, the optimized energy to be almost 26 kcal higher than for the flat configuration (2 TOL up per cell). Thus, while the standing up adsorption configurations might be stable in smaller cavities, flat adsorption is strongly preferred here.

In order to contrast the stability of the pseudo-hexagonal (HEX) structure and the REC structures, we also computed the energy of the HEX structure in contact with vapor. The lowest energy configuration found is shown in Figure 3. It is clear from Figure 3 that there is no room in the HEX lattice for a solvent molecule. The energies per nm<sup>2</sup> of all four optimized structures are compiled in Table 1. The range of experimental values reported for TOL on Au is also given in the table. For myg is the energy for desorption of a molecule from a metal surface to the gas phase at absolute zero and includes the zero point vibrational energy difference.

As Table 1 displays, the SCAN+rVV10 results are consistently lower than the B88vdW values. Both functionals show the desorption energy per unit area for HEX and REC structures to be similar, but the HEX desorption energy per cell is higher (the area of the HEX is 3.60 nm<sup>2</sup> while that of the REC is 4.54 nm<sup>2</sup>). Both functionals show the desorption energy per CoOEP to be similar independent of structure. Both functionals show a significant stabilization of the TCB adsorbed into the REC pocket relative to adsorption on clean Au. The only qualitative difference between the results from the two functionals is that the B88vdW calculation shows toluene more stable in the REC pocket while the SCAN+rVV10 functional has it slightly (0.03 eV) less stable.



**Figure 3:** DFT optimized lowest energy structure found for the HEX CoOEP system on Au(111). As in Figure 1, the bottom two layers of Au used in the calculation have been omitted for clarity. B88vdW functional results.

**TABLE 1:** Energies of desorption transition state for toluene, trichlorobenzene, and cobalt octaethylporphyrin from clean Au(111) and from the REC and HEX structures. The E<sup>0</sup> values include the zero point vibrational energy difference. The experimental range of values for toluene on Au(111) is also given.

	В8	8vdW	SCAN	l+rVV10	B88vdW	SCAN+rVV10	TPD <sup>a</sup>
TCB/Au TOL/Au	E <sub>m/g</sub> 1.055 0.856	E <sub>m/g</sub> /nm <sup>2</sup>	E <sub>m/g</sub> 0.964 0.897	$E_{m/g}$ /nm <sup>2</sup>	E <sup>0</sup> <sub>m/g</sub> 1.015 0.831	E <sup>0</sup> <sub>m/g</sub> 0.924 0.872	0.78-0.90
CoOEP/HEX CoOEP/TCB_REC CoOEP/TOL_REC	5.048 5.178 5.016	2.852 2.925 2.834	4.493 4.593 4.404	2.538 2.595 2.488	4.941 5.071 4.909	4.386 4.486 4.297	
TCB/TCB_REC TOL/TOL_REC	1.426 1.083	3.034 2.304	1.095 0.866	2.329 1.843	1.386 1.058	1.055 0.841	
HEX/Au TCB_REC/Au TOL_REC/Au	10.087 12.343 11.674	2.801 2.721 2.573	9.062 10.873 10.482	2.517 2.397 2.310	9.873 12.049 11.410	8.848 10.579 10.218	

a) from Reference 47

A note on the role of energy per unit area. The calculations of the relative stabilities of the X-REC structure are made easier by the fact that both lattices occupy exactly the same areas on the surface. It is also interesting to note that the electronic energy per nm<sup>2</sup> of the HEX structure is slightly more negative than that for the X-REC structures, making it the most electronically stable structure.

Vibrational Analysis: In order to calculate desorption rates for TCB and TOL, the frequencies of vibration of both the adsorbed TOL and TCB as well as their gas phase values are needed. While the experimental solution phase values are available, the values in the REC structure are not. Thus, we calculated the vibrational frequencies of both TOL and TCB in the REC structure using the B88vdW functional. Because the entire cell is significantly more than 350 atoms, we

did not have the resources to allow every (or even most of the) atom(s) to move. We instead fixed the gold and CoOEP in their optimized positions and then allowed only the TCB or TOL atoms to vary. This procedure is justified by the fact that the changes in the internal modes (the ones most likely to be affected by the adjacent CoOEP hydrogens) relative to the gas phase is small. It is also consistent with a long-standing approximation that internal modes do not change significantly upon physisorption. <sup>48</sup> The gas phase vibrational frequencies were also computed with the same functional and to the same accuracy as the surface frequencies. These computed gas phase values are directly compared to the experimental liquid phase values (Table 2 and 3) as an indicator of the reliability of the calculations. The results of these calculations are presented in Table 2 (TCB) and Table 3 (TOL).

The standard deviations for all but the lowest frequency mode (Calculated gas phase versus experiment in solution) are less than 1.7% for both compounds. One might reasonably expect less agreement with the lowest mode since the calculation is in the gas phase and the experimental value includes interaction with the solvent. Overall, we believe this is excellent agreement for a computation of frequencies that has no adjustable parameters.

TABLE 2: Computed and experimental vibrational frequencies for 1,2,4-trichlorobenzene.

TCB in REC (cm <sup>-1</sup> ) VASP	TCB gas phase (cm <sup>-</sup> 1) VASP	TCB liquid (cm <sup>-1</sup> ) <sup>a</sup>	%err
3138	3141	3094	1.5
3122	3136	3072	2.1
3115	3123		
1558	1556	1571	-0.9
1543	1541	1562	-1.4
1439	1443	1461	-1.2
1371	1363	1377	-1.0
1304	1294	1267	2.1
1245	1240	1245	-0.4

1117       1119       1132       -1.2         1088       1086       1096       -0.9         1015       1019       1036       -1.6         929       934       942       -0.9         871       854       869       -1.8         800       800       817       -2.1         794       787       811       -3.0         672       681       688       -1.0         668       669       679       -1.5         564       572       576       -0.8         536       542       551       -1.6         465       462       456       1.4         438       420       435       -3.5         405       385       396       -2.9         344       323       326       -0.8         295       295       305       -3.4         241       217       212       2.2         212       196       195       0.7         187       175       182       -4.0         144       140       117       19.8         124       110       88       82 <th></th> <th></th> <th></th> <th></th>				
1088       1086       1096       -0.9         1015       1019       1036       -1.6         929       934       942       -0.9         871       854       869       -1.8         800       800       817       -2.1         794       787       811       -3.0         672       681       688       -1.0         668       669       679       -1.5         564       572       576       -0.8         536       542       551       -1.6         465       462       456       1.4         438       420       435       -3.5         405       385       396       -2.9         344       323       326       -0.8         295       295       305       -3.4         241       217       212       2.2         212       196       195       0.7         187       175       182       -4.0         144       140       117       19.8         124       110       88       82	1138	1138	1156	-1.6
1015       1019       1036       -1.6         929       934       942       -0.9         871       854       869       -1.8         800       800       817       -2.1         794       787       811       -3.0         672       681       688       -1.0         668       669       679       -1.5         564       572       576       -0.8         536       542       551       -1.6         465       462       456       1.4         438       420       435       -3.5         405       385       396       -2.9         344       323       326       -0.8         295       295       305       -3.4         241       217       212       2.2         212       196       195       0.7         187       175       182       -4.0         144       140       117       19.8         124       110       88       82	1117	1119	1132	-1.2
929       934       942       -0.9         871       854       869       -1.8         800       800       817       -2.1         794       787       811       -3.0         672       681       688       -1.0         668       669       679       -1.5         564       572       576       -0.8         536       542       551       -1.6         465       462       456       1.4         438       420       435       -3.5         405       385       396       -2.9         344       323       326       -0.8         295       295       305       -3.4         241       217       212       2.2         212       196       195       0.7         187       175       182       -4.0         144       140       117       19.8         124       110       88       82	1088	1086	1096	-0.9
871       854       869       -1.8         800       800       817       -2.1         794       787       811       -3.0         672       681       688       -1.0         668       669       679       -1.5         564       572       576       -0.8         536       542       551       -1.6         465       462       456       1.4         438       420       435       -3.5         405       385       396       -2.9         344       323       326       -0.8         295       295       305       -3.4         241       217       212       2.2         212       196       195       0.7         187       175       182       -4.0         144       140       117       19.8         124       110       88       82	1015	1019	1036	-1.6
800       800       817       -2.1         794       787       811       -3.0         672       681       688       -1.0         668       669       679       -1.5         564       572       576       -0.8         536       542       551       -1.6         465       462       456       1.4         438       420       435       -3.5         405       385       396       -2.9         344       323       326       -0.8         295       295       305       -3.4         241       217       212       2.2         212       196       195       0.7         187       175       182       -4.0         144       140       117       19.8         124       110       88       88         82	929	934	942	-0.9
794       787       811       -3.0         672       681       688       -1.0         668       669       679       -1.5         564       572       576       -0.8         536       542       551       -1.6         465       462       456       1.4         438       420       435       -3.5         405       385       396       -2.9         344       323       326       -0.8         295       295       305       -3.4         241       217       212       2.2         212       196       195       0.7         187       175       182       -4.0         144       140       117       19.8         124       110       88       82	871	854	869	-1.8
672 681 688 -1.0 668 669 679 -1.5 564 572 576 -0.8 536 542 551 -1.6 465 462 456 1.4 438 420 435 -3.5 405 385 396 -2.9 344 323 326 -0.8 295 295 305 -3.4 241 217 212 2.2 212 196 195 0.7 187 175 182 -4.0 144 140 117 19.8 124 110 88 88 82	800	800	817	-2.1
668       669       679       -1.5         564       572       576       -0.8         536       542       551       -1.6         465       462       456       1.4         438       420       435       -3.5         405       385       396       -2.9         344       323       326       -0.8         295       295       305       -3.4         241       217       212       2.2         212       196       195       0.7         187       175       182       -4.0         144       140       117       19.8         124       110       88       82	794	787	811	-3.0
564       572       576       -0.8         536       542       551       -1.6         465       462       456       1.4         438       420       435       -3.5         405       385       396       -2.9         344       323       326       -0.8         295       295       305       -3.4         241       217       212       2.2         212       196       195       0.7         187       175       182       -4.0         144       140       117       19.8         124       110       88       88         82	672	681	688	-1.0
536       542       551       -1.6         465       462       456       1.4         438       420       435       -3.5         405       385       396       -2.9         344       323       326       -0.8         295       295       305       -3.4         241       217       212       2.2         212       196       195       0.7         187       175       182       -4.0         144       140       117       19.8         124       110       88       88         82	668	669	679	-1.5
465       462       456       1.4         438       420       435       -3.5         405       385       396       -2.9         344       323       326       -0.8         295       295       305       -3.4         241       217       212       2.2         212       196       195       0.7         187       175       182       -4.0         144       140       117       19.8         124       110       88       82	564	572	576	-0.8
438       420       435       -3.5         405       385       396       -2.9         344       323       326       -0.8         295       295       305       -3.4         241       217       212       2.2         212       196       195       0.7         187       175       182       -4.0         144       140       117       19.8         124       110       88         82	536	542	551	-1.6
405       385       396       -2.9         344       323       326       -0.8         295       295       305       -3.4         241       217       212       2.2         212       196       195       0.7         187       175       182       -4.0         144       140       117       19.8         124       110         88       82	465	462	456	1.4
344       323       326       -0.8         295       295       305       -3.4         241       217       212       2.2         212       196       195       0.7         187       175       182       -4.0         144       140       117       19.8         124       110       88         82       82	438	420	435	-3.5
295     295     305     -3.4       241     217     212     2.2       212     196     195     0.7       187     175     182     -4.0       144     140     117     19.8       124       110       88       82	405	385	396	-2.9
241     217     212     2.2       212     196     195     0.7       187     175     182     -4.0       144     140     117     19.8       124       110       88       82	344	323	326	-0.8
212     196     195     0.7       187     175     182     -4.0       144     140     117     19.8       124       110     88       82	295	295	305	-3.4
187 175 182 -4.0 144 140 117 19.8 124 110 88 82	241	217	212	2.2
144 140 117 19.8 124 110 88 82	212	196	195	0.7
124 110 88 82	187	175	182	-4.0
110 88 82	144	140	117	19.8
88 82	124			
82	110			
	88			
69	82			
	69			
66	66			

a) Reference 49

TABLE 3: Calculated and experimental frequencies for Toluene in cm<sup>-1.</sup>

_				
	TOL_REC vib VASP	TOL vacuum VASP	Experiment <sup>a</sup> (liquid)	%err
	3106	3118	3067	1.7
	3091	3096	3056	1.3
	3078	3088	3056	1.1
	3072	3085	3039	1.5
	3068	3073	3039	1.1
	3005	3026	2963	2.1
	2985	3006	2933	2.5
	2930	2953	2921	1.1
	1583	1600	1611	-0.7

15

	1562	1576	1585	-0.6
	1487	1496	1500	-0.3
	1458	1473	1463	0.7
	1443	1463	1453	0.7
	1426	1439	1436	0.2
	1375	1377	1384	-0.5
	1327	1331	1330	0.1
	1315	1319	1312 b	0.6
	1205	1201	1212	-0.9
	1182	1174	1178	-0.4
	1161	1162	1155	0.6
	1086	1094	1083	1.0
	1040	1045	1043	0.2
	1024	1028	1030	-0.2
	994	1001	1004	-0.3
	984	990	980	1.0
	973	975	980	-0.5
	955	957	964	-0.7
	886	893	894	-0.1
	840	841	843	-0.2
	787	770	786	-2.0
	730	727	730	-0.4
	690	695	695	0.0
	621	621	623	-0.4
	520	520	521	-0.2
	463	459	462	-0.6
	404	402	405	-0.8
	358	329	341	-3.6
	237	214	205	4.6
	177	119		
	127			
	117			
	104			
	67			
	60			
	35			
- \	D afanan a 50. 1	) D .f.	51	

a) Reference 50; b) Reference 51

The lowest 6 modes for the adsorbed systems are primarily the frustrated rotations and translations. In using these modes to calculate thermochemical properties one must be very cautious of the barrier heights associated with these motions. Low barriers allow the excited

vibrations to become translations or rotations and significantly affect the thermochemical properties. <sup>52,53</sup> Single point calculations were used to estimate the barriers to rotation in the A-B plane. The barrier to a 30-degree rotation in the plane was computed to be 0.89 eV (20.5 kcal/mole) for TCB and about 0.56 eV or 13 kcal/mole for TOL. At room temperature kT is 0.027 eV or 0.5 kcal/mole. McClurg  $^{53}$  has shown that a hindered rotor analysis may be neglected when r = barrierheight/vibrational frequency is large and when kT/vibrational frequency is of the order of 2. The frequencies for all six low energy modes lie between 35 and 127 cm<sup>-1</sup> (0.004 to 0.016 eV). Thus, the frustrated rotations may be treated as vibrations. For the translations in the A-B plane, the molecules are constrained by the adjacent CoOEP and have no option for moving away from equilibrium. In order to question the barrier to hopping out of the cavity and onto the monolayer, we calculated the full potential curve for TCB moving from adsorption to infinity with the plane of the molecule parallel to gold. The result was so interesting that we wound up computing these curves for TOL and TCB on Au only, and for TOL and TCB moving out of the REC pocket (all with B88vdW) and for the TCB-REC case with the SCAN+rVV10 functional. These results will be presented in the next section. For now, we summarize and say that all of the lowest six modes in each molecule may be approximated by a harmonic oscillator. There is an issue with one internal mode of toluene – the "hindered" rotation of the methyl group. Our calculation (see Figure S4) indicates that the barrier to CH<sub>3</sub> rotation on the surface is small, of the order of 280 cm<sup>-1</sup> and the VASP calculated torsional mode (which includes some C-H stretch) is at 177 cm<sup>-1</sup>. Even for this low barrier, the energies and entropies calculated based on a simple harmonic oscillator do not differ significantly at 300K from those calculated for the small barrier limit (eqn 24 in reference 53).

Potential Energy Curves: In order to determine the electronic energy required for desorption, and to better understand the adsorption/desorption process, DFT was used to calculate the electronic energy as a function of distance between substrates and adsorbing molecule (TCB or TOL). Adsorption on Au(111) at low coverage (about 0.2 monolayer of TCB or TOL only) and into the pocket of the REC structure were considered. We first explored the most direct path – the benzene ring maintained its orientation relative to the Au(111) surface [nearly parallel] throughout the process. Figure 4 presents these potential curves for the TCB case, and the results for TOL are given in Figure S5.  $Z_{cm}$  is the z (or C axis) distance between the center of mass of TCB and the top Au plane. Note first that the electronic energy curves are distinctly different for the Au(111) only and the REC/Au case. The TCB on Au(111) data can be readily fit with a Morse potential [shown as the smooth black line in Figure 4].

On the other hand, as TCB approaches the REC/Au(111) surface, one first observes a significant (-0.41 eV) local minimum associated with van der Waals (vdW) interaction with the overall REC layer and repulsion caused by interaction of the (parallel) TCB with the methyl groups surrounding the adsorption site (pocket between CoOEP). The smooth red line in Figure 4 is a cubic spline fit to the calculated points. Figure 4 also provides images of the surface at the extrema of the energy curve. There is a significant increase in energy as the TCB enters the pocket and experiences van der Waals repulsion by the surrounding methyl groups. Once past that point, there is a strong interaction both with the Au substrate and the surrounding CoOEP. The extent of the vdW attractive interaction can be seen in the difference in energy of the TCB on Au(111), only, and on Au(111) in the REC pocket, 0.42 eV. In order to obtain the most accurate possible value for the barrier created by the pocket, a nudged elastic band (NEB) calculation was performed and the barrier was found to be 1.22 eV when the TCB is 0.2 nm above its equilibrium position in the REC

structure. Points from the NEB calculation are displayed as crosses in Figure 4. The TOL on REC potential curves are qualitatively the same (Figure S5), but the depth of the pocket potential is somewhat less.

The SCAN+rVV10 functional also shows the effect of the methyl group repulsion (Figure S6). Single point calculations clearly exaggerate the effect of methyl group repulsion. Thus, we performed another set of calculations where the entire adlayer (except for the TCB lifted from the surface) could relax to its minimum energy position. As expected, the size of the barrier was significantly reduced, but is still present.

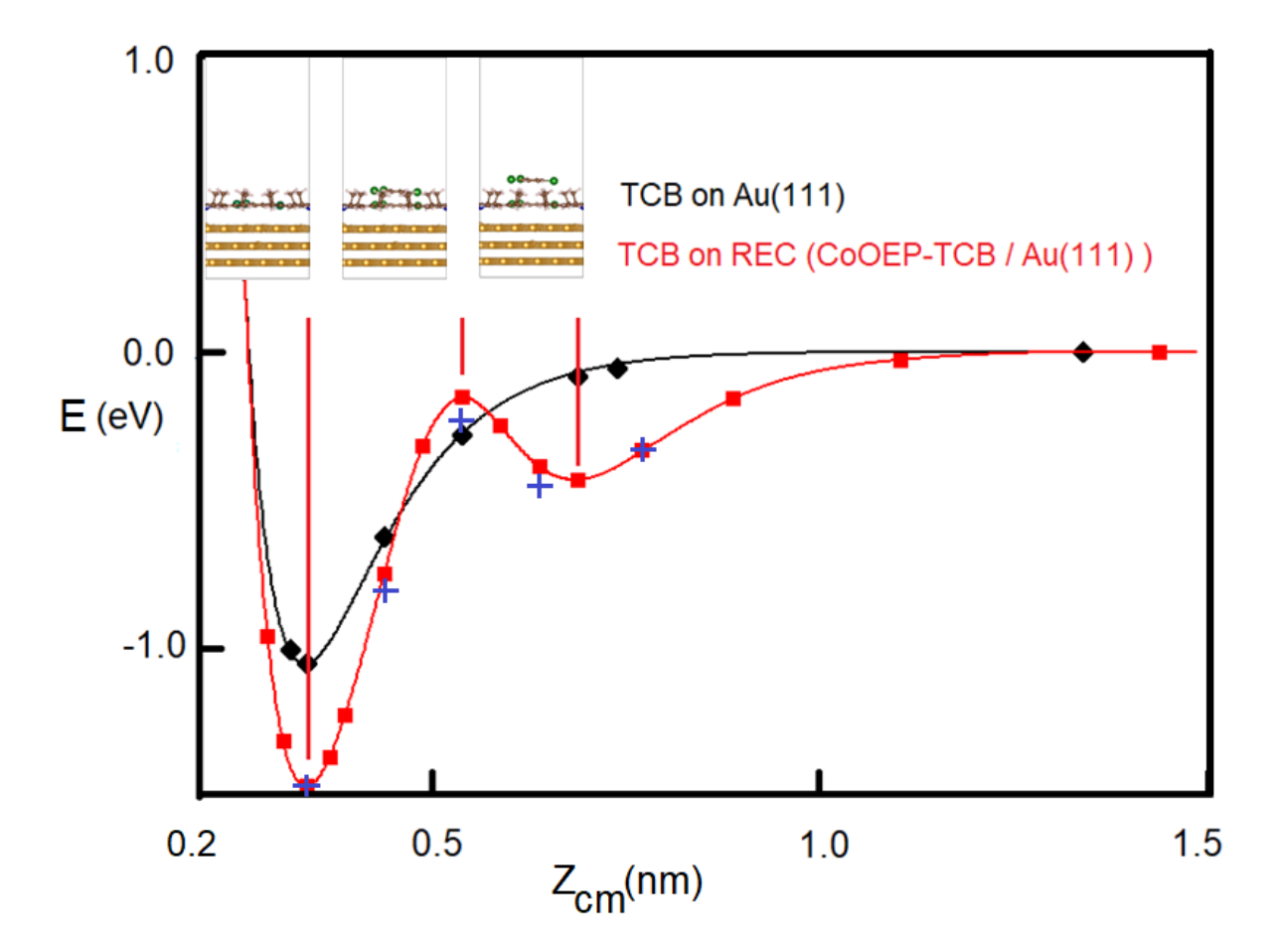


Figure 4. DFT calculated electronic energy curves as a function of distance from the top Au plane to the center of mass of TCB ( $Z_{cm}$ ). TCB was held parallel to the Au(111) plane at all distances. Red curve: Electronic energy as TCB adsorbs into the pocket in

the REC structure. Insets show configuration of TCB relative to the REC structure at three extrema. Blue Crosses: NEB calculated potential for TCB parallel orientation absorption. Black curve: Electronic energy as a function of  $Z_{cm}$  for TCB adsorbing on Au(111), only, at an effective coverage of about 0.2 monolayer.

The strong repulsive nature of the TCB (parallel) – methyl interactions, and the additional adsorption energy provided by vdW interactions in the REC pocket, justify consideration of a standing adsorption into the pocket. We chose the most stable configuration of standing TCB on Au(111), the Cl-H-Cl down configuration shown in Figure 5. The electronic energy as a function of Z<sub>cm</sub> for this case is shown superimposed on the parallel adsorption curves in Figure 5. As in the parallel adsorption case, the potential cannot be fit by a Morse curve, and shows a clear initial vdW interaction with the REC adlayer at long distances. Unlike the parallel case, it is possible to orient the TCB to essentially eliminate the CH<sub>3</sub> repulsion part of the curve, as show in Figure 5. The optimized equilibrium structure at the minimum in the blue curve in Figure 5 is shown in Figure S7. The optimized TCB-REC structure is shown for comparison in Figure S8. The similarity in minima of the blue curve (standing TCB in REC pocket) and the red curve (flat TCB on Au(111)) results from an accidental cancelation in the greater adsorption energy of the parallel case on Au with the vdW stabilization of standing TCB in the REC pocket.

The blue curve in Figure 5 cannot represent final true adsorption curve. At some point when  $Z_{cm} \lesssim 0.5$  nm TCB must begin to turn parallel to the surface in order to find the most stable configuration as shown in Figure 1.

Actually, this discussion about the variation in barrier shape is of interest only in terms of the detailed kinematics. The Eyring theory result we will use is independent of the shape of the barrier

so long as it doesn't change the surface vibrational partition function significantly. There could be several local minima in one path, none in another, and yet a different shape in the nth path and the same desorption rate would result. An alternative way of stating this is: "In TST derivations, the rate is calculated assuming that the initial state is in equilibrium with the TS. As long as the initial state and transition state keep the same local Potential Energy Surface, you can change the PES by huge amounts in between without any effect on the TST rate." <sup>54</sup>

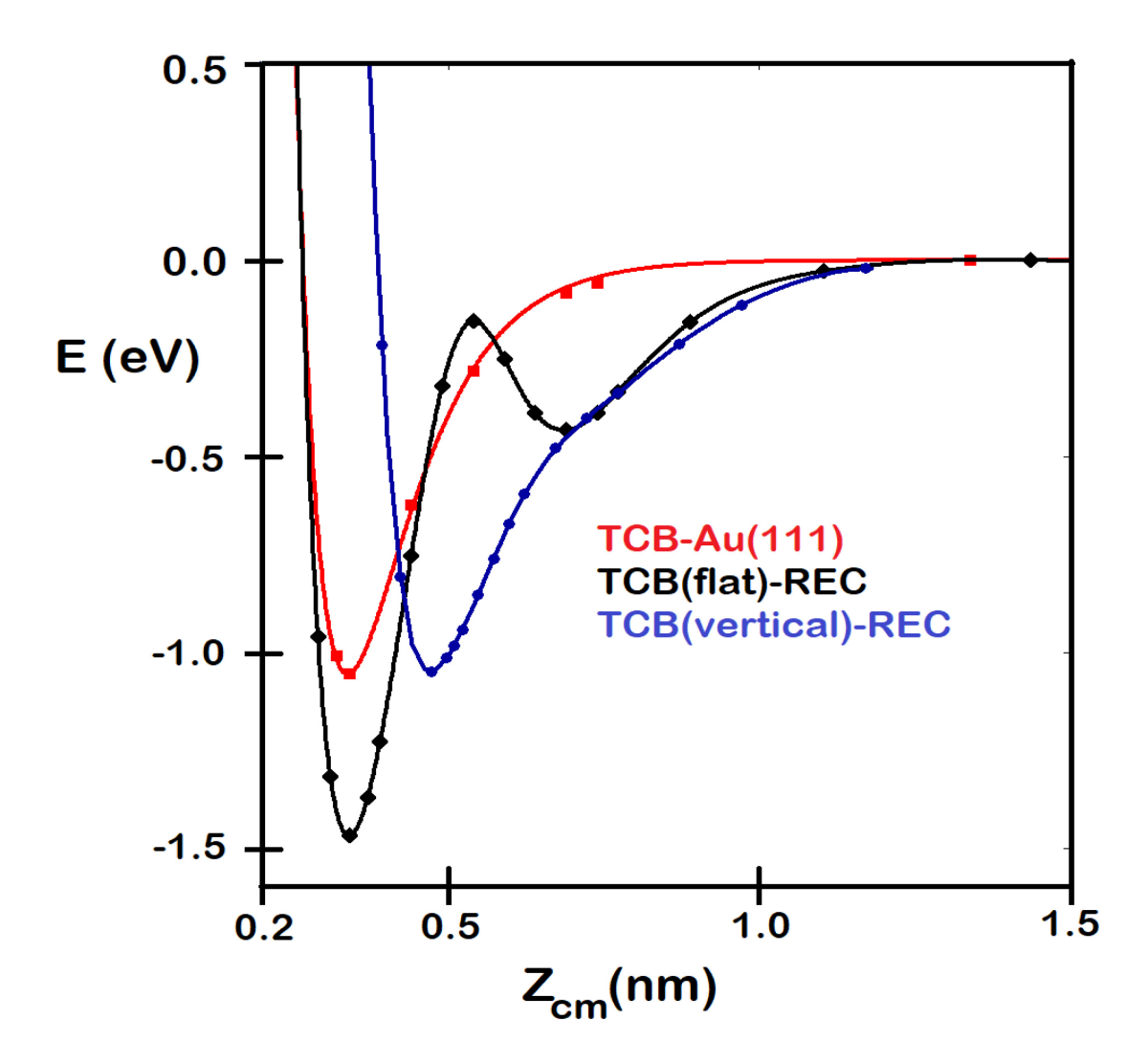


Figure 5. DFT calculated potential energy curves as a function of distance from the top Au plane to the center of mass of TCB ( $Z_{cm}$ ). Black curve: Electronic energy as TCB

adsorbs into the pocket in the REC structure. Red curve: Electronic energy as a function of  $Z_{cm}$  for TCB adsorbing on Au(111), only, at an effective coverage of about 0.2 monolayer. Blue curve: Electronic energy as TCB adsorbs into the pocket in the REC structure but oriented vertically with the CI-H-CI down configuration that gives the most stable vertical structure on Au(111).

**Kinetics:** Given the electronic and zero-point vibrational energy difference between the adsorbed state and the transition state, one can use Eyring reaction rate theory <sup>44,55-57</sup> to calculate desorption rates. All kinetic values will be calculated either at 298K or at 408K, as indicated in the tables. It must first be noted that the REC and HEX structures are clearly a 2-D lattice gas system and must be treated as such. Campbell <sup>56</sup> gives the desorption rate per unit area for a 2-D lattice gas, and we have scaled it to monolayers/minute where N<sub>m</sub> is the number of molecules per monolayer.

$$\frac{R}{A} = \kappa \left(\frac{kT}{h}\right) \left(\frac{2\pi mkT}{h^2}\right) \left(\frac{q_{TSint}}{q_{ad}}\right) \left(\frac{\theta}{1-\theta}\right) \exp\left(\frac{-\Delta E_d^0}{kT}\right) \left(\frac{60}{N_m}\right) \quad \text{eqn 1}$$

Where  $q_{TSint}$  is the partition function for the rotational and vibrational modes of the molecule of interest in the gas phase,<sup>58</sup> and  $q_{ad}$  is the partition function for a single adsorbed molecule in the lattice.  $\Delta E_X$  is the DFT calculated electronic desorption energy for species X,  $\Delta E^0_d = E_X - \Delta E_{0p,X}$ , and  $\Delta E_{0p,X}$  is the differences in zero point vibrational energies and can be found in **Table S1**. That is,  $\Delta E^0_d$  is the difference between the zero-point energies of the molecule in the transition state and the adsorbed molecule.

$$qv_i = \frac{1}{1 - \exp\left(\frac{-hv_i}{kT}\right)}$$

$$q_{TSint} = \frac{1}{\sigma} \left( \frac{\pi T^3}{AXBXCX} \right)^{1/2} \prod_{i=1}^{3N-6} qv'_i$$
$$q_{ad} = \prod_{i=1}^{3N} qv_i$$

Where  $\sigma$ =1 for Toluene and for TCB and 4 for CoOEP.  $\kappa$  is the transmission coefficient of the order of 1. The frequency of a normal mode is given by  $\nu_i$ , and AX, BX and CX are the rotational temperatures for the free molecule X. While the zero-point energies are quite large, their differences are small, of the order of 40 meV, or about 5% of the electronic desorption energy of TOL and TCB.

Using these relationships and the values reported above and in Tables 1, 2, 3 and S1, one can compute the desorption rate/cm<sup>2</sup> for toluene or trichlorobenzene leaving the pocket of the REC structure at 298K in the gas phase.

$$\frac{R}{A}(\theta, TCB) = 0.027 \frac{\theta}{1-\theta}$$
 Monolayers/minute eqn 2

$$\frac{R}{A}(\theta, TOL) = 4.5x10^2 \frac{\theta}{1-\theta}$$
 Monolayers/minute eqn 3

Treating CoOEP is more difficult. Because of the size of the system, and the propagation of errors for the huge number of low frequency bands, we did not attempt to calculate all the vibrational frequencies on the surface. Instead, we relied up the long-standing approximation that internal modes do not change significantly upon physisorption.<sup>48</sup> This should work for all but the CH<sub>2</sub> wag (torsional) modes of the ethyl groups which are severely constrained upon adsorption. Also, an approximate treatment of the 6 lattice modes is required. These two sets of motions are discussed and partition functions are derived in the SI. With these approximations,

$$\left(\frac{q_{TSint}}{q_{ad}}\right) = q_{tor}/q_{lat}^{Co}$$

$$\frac{R}{A}(\theta, CoOEP, TOL - REC) = < 1.0x10^{-50} \frac{\theta}{1-\theta}$$
 Monolayers/minute at 298K eqn 4

$$\frac{R}{A}(\theta, CoOEP, TCB - REC) = <1.0x10^{-50} \frac{\theta}{1-\theta}$$
 Monolayers/minute at 298K eqn 5

$$\frac{R}{A}(\theta, CoOEP, HEX) = <1.0x10^{-50} \frac{\theta}{1-\theta}$$
 Monolayers/minute at 298K eqn 6

This negligible rate of desorption into the gas phase at 298K is a primary contributor to the kinetic stability of all three lattices. Once a CoOEP adsorbs from the vapor onto the surface, it may slide around, but it isn't coming off.

Note first that the desorption rate for TCB into the vapor is about 4 orders slower than for toluene. Also, note that the desorption rate depends upon coverage and accelerates considerably for  $\theta$  greater than about 0.8. How do these results relate to kinetics of the REC to HEX conversion? The rate of desorption from the HEX pocket is only physically important so long as the pocket is maintained. Using the area per CoOEP in the HEX structure (1.80 nm²), and assuming it is the same in REC, one finds that for both TOL and TCB the area per pocket is  $0.47\pm0.01$  nm². Thus, to open a hole large enough to accommodate a single CoOEP molecule, four TCB or TOL must leave the REC structure. Further, the departing molecules must be close enough together in space to allow neighbors to rearange, or CoOEP to adsorb, into the cavity. In the case of vapor-surface equilibrium, or liquid surface equilibrium (to be discussed later) the events must also be close in time so that one or more of the pockets is not filled by an adsorbing solvent molecule. Each CoOEP has 4 TOL or TCB nearest neighbors. It seems reasonable to assume that the loss of these four TOL or TCB is the primary mechanism for creating an opening. Assuming desorption occurs

randomly on the surface, the probability that the four adjacent sites will be vacant at TCB or TOL coverage  $\theta$ , is P44( $\theta$ ) i. P44( $\theta$ ) are given by:

$$P44(\theta) = \sum_{n=4}^{4} \frac{k!}{n!(k-n)!} \theta^{k-n} (1-\theta)^n$$
 eqn 7

This function is shown in Figure S9 of the SI. During the initial phase of desorption of solvent from the REC form (we define  $\theta$ =0.95 as the initial state), P44(0.95) =  $6x10^{-6}$ . This factor reduces the rate of conversion from the rate of TOL or TCB desorption, In fact, one must include additional reductions due to diffusion and rotation rates of the CoOEP on the surface, (there is no adsorption of CoOEP in the case of vacuum or equilibrium vapor exposure of solvent at 298K) as they move into the HEX positions. Thus, the rates given in equations 2 and 3 are upper limits for the rate of REC to HEX conversion in vacuum or vapor. Whatever the mechanism for REC to HEX conversion, it can never proceed faster than the rate at which the solvent is lost from the REC structure.

Surface Solution Interface: It is clear that the TCB-REC structure is significantly more stable than the TOL-REC structure in contact with vapor, and that there is a huge kinetic barrier for the conversion of the TCB-REC to HEX structure. More problematic (and interesting) is the situation when these structures are in contact with solvent. In order to address the role of solvent on the critical issues energy change on desorption (and therefore equilibrium state) and to gain insights about the activation energy and the kinetics of desorption in contact with solvent, we will use a method proposed by C. T. Campbell for estimating the difference in adsorption energy of a molecule in the presence and absence of a liquid solvent. This model assumes pairwise interfacial bond additivity (e.g., that the bond energy of the molecule to the surface is the same with or without solvent molecules interacting with other parts of the molecule). <sup>28-29</sup> Following his approach to the

problem requires two major steps. First, we must find the adhesion per unit area of the solvent to the solid surface. -- the work required to separate a unit area of wetted surface into a liquid surface and clean solid surface. The second step in Campbell's treatment was to find the difference in adsorption/desorption energy in gas phase versus under a liquid solvent by creating a sequence of steps whose sum total yielded the desorption energy of an adsorbate into solution. As presented in the Supplemental Power point, we extend his derivation to define the critical quantities in terms of per molecule. This extension requires that there is a narrow distribution of adsorption geometries and energies. This assumption is justified for the cases considered here, but may fail for more poorly defined systems. Thus, we use  $\Delta e$  to represent the change in energy per molecule rather than the change in energy per unit area in the original Campbell treatment. We stress that this is the difference in energy between final and initial states and not the activation energy.

Let us first consider the adhesion energy. Adhesion energy of the solvent to a metal surface can be expressed in terms of the gas phase desorption energy,  $\Delta e_{des,g}$ , the energy of vaporization,  $\Delta e_{vap}$  of the solvent, and the energy require to form the (planar thin) solvent surface layer,  $2\sigma e_{l/v}$ , all per molecule of solvent in contact with the surface. Where  $\sigma$  is the area of the solvent in contact with the surface. In his papers, Campbell set  $e_{l/v} = \sigma \gamma$ , where  $\sigma$  is the area of the surface occupied by a solvent molecule and  $\gamma$  is the surface tension of the solvent per unit area of the surface. This formulation neglects the entropic contribution which turns out to be sizable. The correct form is  $e_{l/v} = \sigma(\gamma - T(d\gamma/dT))$ , where  $(d\gamma/dT)$  is negative for most solvents. The result is:

$$\Delta e_{adh} = \!\! \Delta e_{des,g} \text{ - } \Delta e_{vap} + \!\! 2\sigma [\gamma \text{-} T (d\gamma/dT)].$$

# Derivation of this result and of equations 8 and 9 are given in the SI Power Point.

Recognizing that the desorption energy is the DFT calculated desorption energy including zero point vibrational energy,  $E_{m/g}^0$ , plus the thermal energy of the gas minus the thermal energy of the

adsorbed solvent, gives,  $\Delta e_{des,g} = E^0_{m/g} + 3kT + \Delta e_v$ . Where we have assumed a non-mobile adsorbate and that  $\Delta e_v$  is the difference in vibrational energy for the adsorbed and gas phase molecule and the solvent is assumed to be non-linear. Thus, the energy of adhesion of the solvent to a generic metal surface is:

$$\Delta e_{adh} = E_{m/g}^{0} + 3kT + \Delta e_{v} - \Delta e_{vap} + 2\sigma \left[ \gamma - T \left( \frac{d\gamma}{dT} \right) \right] \qquad \text{eqn } 8$$

The energies of vaporization at 298K and 408K needed for eqn 8 were found using the Antoine equation. This thermodynamic data and other needed thermodynamic quantities can be found in the SI.

The second step in Campbell's treatment was to create a sequence of steps whose sum total yielded the desorption energy of an adsorbate into solution. This sequence of steps is mostly thermodynamically sound, but it has two approximations: 1) The adsorbate is somewhat flat; 2) the energy of wetting the adlayer is the sum of the work returned when the liquid surface disappears and half the solvation energy of the adsorbate. He later expanded on his treatment to include more complex adsorbate shapes, <sup>60</sup> but the original treatment suffices for the molecules considered here. Details of our corrected derivation are given in the SI power point. The end result is:

$$E_{A,m/S}^{0} = E_{A,m/g}^{0} - \left(\frac{\sigma_{A}}{\sigma}\right) \Delta e_{adh,S} + \frac{\Delta e_{A,S}}{2} + \sigma_{A} \left[\gamma - T\left(\frac{d\gamma}{dT}\right)\right] \quad \text{eqn } 9$$

Where  $E_{A,m/S}^0$  is the desorption energy (including zero point vibrational energy) for desorption of A from a metal surface into solvent S,  $E_{A,m/g}^0$  is both the desorption and transition state energy for desorption of A from a metal surface into the gas phase, and  $\Delta e_{A,S}$  is the solvation energy of adsorbate A. It turns out that the correction can be quite large and reduces  $E_{A,m/g}^0$  by more than half for CoOEP in Au(111). Table 4 presents the values of  $E_{A,m/S}^0$  and  $E_{A,m/g}^0$  for the various

structures of CoOEP in TOL and TCB as computed both by B88vdW and by SCAN+rVV10. Table S2 provides values at 298K and 408K and also adds values computed using the Tkatchenko-Scheffler functional.

Because the desorption energies of the solvents differ significantly between desorption from clean gold and desorption from the REC pocket, two different energies of adhesion result for each solvent. In the case of desorption of solvent from the REC pocket, it was clear that the REC pocket desorption energies should be used to calculate the adhesion energies. For CoOEP or a full REC cell, however, the choice is less clear since about 4 solvent molecules are required to fill the CoOEP space. We chose to use the solvent adsorption on clean gold values for the solvent adhesion energy when considering CoOEP or REC cell desorption.

A more difficult issue is the difference in transition state and final state energies for desorption into solution. Because the final state is a fully solvated molecule, and the transition state may not be, the transition state is usually higher in energy that the final desorbed state. Thus, the true transition state energy in solution lies somewhere between the gas phase desorption energy and the solution phase desorption energy. As an example, consider a transition state where the CoOEP retains the partial solvation it had on the surface but has moved ~ 1 nm from the Au but that the Au has not become solvated. At this point the zero-point desorption energy would be of the order of the desorption energy for the gas phase plus one half the solvation energy. For CoOEP in TOL the solvation energy is calculated in the SI to be -0.67 eV/molecule. This hypothetical scenario would put the solution phase activation energy at 0.34 eV lower than the gas phase transition state but significantly higher than the zero-point desorption energy difference in TOL. Alternatively, one might imagine that the transition state was a solvated Au surface and a partially solvated CoOEP. In this case the activation energy for desorption would be about 0.4 eV more than the

desorption energy. We will therefore compute desorption rates using gas phase transition state energies and solution phase desorption energies in order to set limiting values for rates. *The initial desorption rates presented in Table 4 are the limiting values with the true desorption rate laying somewhere between the two.* We note for future reference, that when calculating equilibrium properties, the desorption energies (not the transition state energies) are the correct values and no such difficulty arises.

With values for the limiting desorption activation energies in hand, we can use equation 1 to estimate the limiting desorption rates of CoOEP into either TCB or TOL at 298K and 408K. Note that this is an initial rate ( $\theta = 0.95$ ) and the units are monolayers per minute. We have chosen the 408K temperature because the only data on desorption rates for CoOEP into solution that we know of is for the HEX form desorbing into n-octylbenzene. <sup>61</sup> Thus, we have a point of comparison. The calculated desorption rates both to the vapor and into solution are tabulated in Table 4. It is useful to note that a 2.34 eV activation energy produces a CoOEP desorption rate value of 3 x10<sup>-3</sup> monolayers/min in both TCB and TOL at 135°C

TABLE 4: Limiting values for the initial rate of desorption (monolayers/min) for the indicated species in the indicated environment: species [environment]. B88vdW vibrational energy values, and corrections for solvent as discussed in the text.  $\theta$ =0.95. See discussion in text concerning why the actual desorption rates in solution are intermediate between the vapor and solution phase values given here.

	SCAN+rVV10				
	eV/molecule		Initial Rate (monolayers/m		min)
T = 298K	$E^0_{m/g}\left[REC\right]$	$E^0_{m/s}\left[REC\right]$	[REC, g]	[REC, TCB(l)]	[REC, TOL(l)]
TCB	1.055	0.843	$1.0 \times 10^6$	$4.0x10^9$	
TOL	0.841	0.792	$1.9x10^{8}$		$1.3x10^9$
CoOEP [TCB-REC]	4.486	2.055	$4.8x10^{-50}$	$6.3x10^{-9}$	
CoOEP [TOL-REC]	4.297	1.522	$7.6 \times 10^{-47}$		6.47

T=298 K	$E^0_{\ m/g\ [HEX}]$	$E^0_{m/s}$ [HEX]	[HEX, g]	[HEX, TCB(1)]	[HEX, TOL(1)]
CoOEP [TCB]	4.386	1.955	$1.9x10^{-48}$	$2.4 \times 10^{-7}$	
CoOEP [TOL] T= 408 K	4.386	1.611	1.9x10 <sup>-48</sup>		0.16
CoOEP [TCB]	4.386	2.018	$1.5 \times 10^{-28}$	28	
CoOEP [TOL]	4.386	1.666	$1.5 \times 10^{-28}$		$6.3x10^5$
CoOEP [PhO]		a			${4x10^{-3}}$ a
			B88-vdW		
	eV/mo	olecule		Rate (monolayers/	/min)
T = 298K	${ m eV/mc}$ ${ m E^0}_{ m m/g} [{ m REC}]$	blecule $E^0_{m/s} [REC]$		Rate (monolayers/[REC, TCB(l)]	/min) [REC, TOL(l)]
T = 298K TCB			Initial	, ·	•
	$E^0_{\ m/g}\left[REC\right]$	$E^0_{\ m/s}\left[REC\right]$	Initial [REC, g]	[REC, TCB(l)]	•
TCB	$E^{0}_{m/g}$ [REC] 1.386	$E^{0}_{m/s}$ [REC] 1.173	Initial [REC, g] 2.6	[REC, TCB(l)]	[REC, TOL(l)]
TCB TOL	$E^{0}_{m/g}$ [REC] 1.386 1.058	E <sup>0</sup> <sub>m/s</sub> [REC] 1.173 1.009	Initial [REC, g] 2.6 4.0x10 <sup>4</sup>	[REC, TCB(l)] 1.0x10 <sup>4</sup>	[REC, TOL(l)]

[HEX, g] <10<sup>-50</sup>

<10-50

 $2.2x10^{-35}$ 

2.2x10<sup>-35</sup>

[HEX, TCB(l)]

 $6.3x10^{-11}$ 

0.2

 $\{10^{-3}\}^a$ 

[HEX, TOL(1)]

 $1.4x10^{-13}$ 

 $2.8 \times 10^{-3}$ 

 ${4x10^{-3}}$ a

 $E_{m/s}^{0}$  [HEX]

2.167

2.324

2.192

2.342

a) This rate of desorption was determined experimentally in ref 61.

 $E^0_{m/g[HEX]}$ 

4.941

4.941

4.941

4.941

T=298 K

T = 408 K

CoOEP [TCB]

CoOEP [TOL]

CoOEP [TCB]

CoOEP [TOL]
CoOEP [PhO]

There are several observations one may make regarding the data in Table 4. The first is that CoOEP is essentially stuck on the surface at room temperature while the adsorbed TOL and TCB are readily exchanging with either gas or solution. Second is the dramatic reduction in the desorption energy of CoOEP in solution relative to the gas phase. The combination of solvation energy, and solvent adhesion energy reduces the desorption energy by more than a factor of 2. In this context one might note the much smaller reduction of the TOL and TCB desorption energy in

solution relative to CoOEP. A major contributor to this difference is the fact that one must wet the gold surface with almost four molecules of solvent to replace one CoOEP desorption, but only one for TCB or TOL desorption. The third major observation is that both DFT functionals predict that the TCB desorption rate from the REC structure will be less than that for TOL, both in the gas phase and in solution. Fourth, as mentioned above, a 2.34 eV activation energy produces a CoOEP desorption rate value of 3x10<sup>-3</sup> monolayers/minin both TCB and TOL at 135°C. The fact that this is the B88vdw calculated value for the desorption energy for CoOEP in TOL at 135°C, may be accidental since it would imply an activationless adsorption. On the other hand, the values determined from the SCAN+rVV10 functional imply an activation energy ranging from 0.32 to 0.67 eV. These values are well within corrections associated with solvation effects.

Before leaving the subject of computed rates, one must realize how sensitive the rates are to small changes in the activation energy. At 408 K, a change in the activation energy of CoOEP by 0.10 eV (5%) results in a change in the desorption rate by a factor of 10. The DFT calculated CoOEP desorption energies vary by more than 10% depending on the functional chosen. Thus, small errors in the computed energy result in large variations in desorption rate. Even given a perfectly computed desorption energy into the vapor, the energies of solvation for CoOEP in TCB and TOL are based on values with rather large error bars, especially in the TCB case. They could also contribute errors of order 0.1 eV/molecule to the desorption energy into solution. Errors in the vibrational partition functions for CoOEP resulting from the approximations used could produce a change of one or two orders of magnitude in the rate. Beyond these possible variations, there is the issue of the unknown activation energy. Simple partial solvation models (vide supra) suggest that the activation energy for adsorption should be at least 0.4 eV. An empirical fit of the calculated desorption rates for CoOEP in TOL or TCB at 135°C suggests that the smaller

desorption energy values obtained with SCAN+rVV10 functional may be more accurate since they imply an activation barrier to adsorption of 0.3 to 0.7 eV.

Campbell<sup>62</sup> has given a formula for the rate of impingement of solution phase molecules on a surface.

$$J = C * \sqrt{\frac{kT}{2\pi m}}$$

If k is the Boltzmann constant, m is the mass per molecule of the solvent, and C is the concentration of the solvent in molecules/cm<sup>3</sup>, then J has units of molecules/cm<sup>2</sup>-s. For convenience, this can be converted to J $\theta$ , the number of monolayers/minute impacting the surface. Where Nm is the number of sites for solvent adsorption per cm<sup>2</sup>, and is  $4.41 \times 10^{13}$  for TOL or TCB into REC sites.

$$J\theta = C * \sqrt{\frac{kT}{2\pi m}} \left(\frac{60}{Nm}\right)$$

 $J\theta$  is  $(4\pm1)x10^{13}$  monolayers/min for either solvent. Thus, even if the sticking coefficient was as small as  $10^{-7}$ ,  $^{62}$  the replacement rate of solvent into the emptied pores would be much greater than the rate of pore opening for the B88vdW result.

We recently measured the diffusion coefficient, D, for the double decker phthalocyanine, Y[C<sub>6</sub>S-Pc]<sub>2</sub>, on gold in phenyloctane. We found a value of  $1.1x10^{-3}$  nm<sup>2/sec</sup> for D. If the CoOEP (assuming the same diffusion coefficient) must diffuse about 0.5 nm to block re-adsorption of the solvent and start conversion of the Rec to Hex form, it would take about 2 minutes on average. Even if CoOEP diffuses  $10^4$  times faster than Y[C<sub>6</sub>S-Pc]<sub>2</sub>, that is still many orders of magnitude longer than the time required for a solvent molecule to refill the open site and block its motion at 298K. These rates for emptying and filling pores, combined with the relatively slow diffusion rate of CoOEP on Au at 298 support a kinetically limited model for the REC to HEX conversion.

**Thermodynamic Equilibrium in Solution:** The equilibrium requirement for conversion of a complete monolayer of the X-REC structure to the HEX in the presence of both X and CoOEP is:

$$(\beta - 1)\mu_{CoOEP}(M) + \frac{\mu_{X-rec,X}}{2} = \beta \frac{\mu_{hex,X}}{2} + \mu_X(M')$$
 eqn 10

Where  $\mu_{x\text{-rec},X}$  is the chemical potential of a unit cell of the X-REC structure in contact with solvent X,  $\mu_{\text{LeoOEP}}$  (M) is the chemical potential of CoOEP at some molarity, M, and  $\mu_X$  is the chemical potential of X at some molarity M'.  $\beta$  is the ratio of unit cell areas of REC to HEX and is equal 1.260. This is a very different process than the ones considered previously since the number of CoOEP on the surface must increase to compensate for the change in surface density. While we can write an expression for the equilibrium constant for this process, it is highly unlikely to occur as an equilibrium process in the vapor, since CoOEP has no significant vapor pressure below about 250 °C  $^{63}$ , where the TOL or TCB would evaporate from the surface. This process can occur in solution. We will assume the case where the volume of solution is sufficiently large that the equilibration on the surface does not effectively change the concentration in solution. Further, the solvent is assumed to be the reagent TOL or TCB for TOL-REC and TCB-REC, respectively.

We can use the same process used earlier to estimate the desorption energies for the unit cell desorption in the presence of solvent. These results are given in Table 5. Note that unlike the rate calculation, it is the difference in initial and final states ( $E^0_{m/g}$  and  $E^0_{m/g}$ ) not activation energies that are needed here.

Let us continue to assume that the internal vibrations do not significantly change and that the one mole/L standard state is used for all solutions in eqn 10. Further we assume that the partition

functions for the components of the REC cell are the product of the partition functions for the individual components. Using the assumptions used in the previous section, we have:

$$\left(\frac{M_{Co}}{M^0}\right) \cong \left(\frac{q_T^{0,Co}q_r^{Co}q_{tor}}{q_{lat}^{Co}}\right) \left[\left(\frac{q_T^{0,X}q_r^X}{q_{lat}^X}\right) \left(\frac{M^0}{M_X}\right) \exp \left\{\frac{\left(\beta E^0_{Hex,X} - E_{REC,X}^0\right)}{2kT}\right\}\right]^{\frac{-1}{\beta-1}} \qquad \text{eqn } 11$$

Where  $M_{Co}$  is the molar concentration of CoOEP in X when the REC and HEX forms are in equilibrium, the Co notation is shorthand for CoOEP and the superscript 0 on the translational partition functions refers to the 1 mole/L standard state. Na is Avagadro's number, and  $q_T^0 = \left(\frac{2\pi mkT}{h^2}\right)^{3/2} \left(\frac{10^3 r}{Na}\right)$  where r is a factor less than or equal to 1 used to account for the actual free volume within the solution.<sup>48</sup> There have been many proposals for how to determine r,<sup>48,64</sup> with values ranging from 1 down to less than  $10^{-4}$ . The factor r reduces the entropy of desorption but does not affect the desorption energy.

TABLE 5: Desorption energies for the indicated species in the indicated environment: species [environment].

			SCAN+rVV10	
	eV/ur	nit cell		eV
T = 298K				
	$E^0_{REC/g}$	$E^0_{REC/s}$		$\beta E^0_{HEX/s}$ - $E^0_{REC/S}$
[TCB]	10.579	4.131		
[TOL]	10.218	3.025		
	$\rm E^0_{HEX/g}$	$E^0_{HEX/s}$		
[TCB]	8.848	3.985		0.890
[TOL]	8.848	3.297		1.129
			B88vdW	
	eV/ur	nit cell		eV
T = 298K				
	${\rm E^0_{REC/g}}$	$\rm E^0_{REC/s}$		$\beta E^0$ <sub>HEX/s</sub> - $E^0$ <sub>REC/S</sub>
[TCB]	12.01	4.697		

[TOL]	11.343	4.547	
	$\mathrm{E^0_{m/g}}[\mathrm{HEX}]$	E <sup>0</sup> <sub>m/s</sub> [HEX]	
[TCB]	10.341	4.792	1.885
[TOL]	10.341	5.105	1.341

If one inserts the value from Table 5 into eqn 11 and takes r equal to any value between 1 and  $10^{-4}$ , the resulting values of the molarity of CoOEP required to sustain equilibrium are impossibly small (less than 1 molecule / liter!). In fact, so long as  $\beta E^0_{HEX/s}$  -  $E^0_{REC/S} > 0$  and  $r \ge 10^{-3}$ , the HEX form will be the thermodynamic equilibrium form in TCB so long as  $M_{Co} > 10^{-8}$  moles/L. . *Thus,* the REC structures are entirely kinetically driven. This is a very robust conclusion since  $\beta E^0_{HEX/s} - E^0_{REC/S} > 0.9$  for both methods of computation.

#### **CONCLUSIONS**

Computational chemistry was used to explore the kinetics and thermodynamics of the transformation of a solvent incorporated pseudo-polymorph into a unique single component monolayer. DFT calculations of the electronic and vibrational energies of these systems were performed on the system in contact with the gas phase and it was found that the HEX structure was the most energetically stable on the basis of energy per unit area on the surface. The desorption energies into solution were estimated using a model first proposed by Campbell and slightly modified here. The use of these gas phase transition state energies and solution phase adsorption energies allowed for the calculation of limiting rates of desorption. The same adsorption energies allowed computation of equilibrium properties for the systems in contact with solvent.

Rates of desorption from the REC structure of two common solvents (toluene and 1,2,4-trichlorobenzene) were contrasted and it was found that they differed by several orders of

magnitude in the vapor phase, but that the difference was significantly reduced in solution. Considering that TOL and TCB are of similar size and both have the similar  $\pi$  structure, why would one be more stable than the other? The primary driver for the difference in stability of the pseudo-polymorphs was the difference in electronic adsorption energies and the associated increased desorption rate of toluene versus TCB. Moreover, it was found that both the energy of adsorption of the solvent onto substrate and the intermolecular interactions of the solvent with the surrounding tectons must be considered. The energy of adsorption of the solvent onto the substrate in the absence of the second component cannot account for the stability of the binary system. This is a fundamentally important observation that should apply to any host-guest system.

The equilibrium thermodynamic concentration of CoOEP in solutions of either TOL or TCB were calculated by statistical mechanical methods. It was found that the HEX form is the equilibrium form at all practical concentrations at room temperature. Thus, the REC structures are kinetically driven structures. We suggest that the more rapid rate of desorption of TOL from the TOL-REC lattice (traceable to its lower adsorption energy) is what makes the TOL-REC structure less stable than the TCB-REC structure.

It was also discovered that the orientation of adsorbing molecules plays a significant role in determining the potential energy surface for adsorption when the host molecules are not completely planar. In this case, the small 'crown' of CH<sub>3</sub> groups surrounding the porphyrin cores was enough to significantly affect the shape of the potential energy curves for different solvent adsorption trajectories. Interestingly, orientational dependent changes in the adsorption potential energy curve have no effect on the desorption rate calculated using Eyring's reaction rate theory.

Two different DFT functionals were used in this calculation and the corresponding desorption energies varied significantly ( $\sim$ 14%). The computed corrections to the desorption energies due to

solvent wetting were large, of the order of 50% of the gas phase electronic energies. The computed rates were extremely sensitive to the transition state energy values, varying an order of magnitude with a 5% change in the transition state energy at 298K. Moreover, the activation energy for adsorption from solution was not included in the calculation. Thus, the rates calculated in Table 4 should be viewed as limiting values, not quantitative values. The SCAN+rVV10 adsorption energy values, when modified to obtain an estimate for the activation energy, seem most consistent with the known REC desorption rate at 135°C. The conclusion that the HEX structure is the thermodynamically stable structure at all practical concentrations of CoOEP, on the other hand, is robust.

#### **AUTHOR INFORMATION**

The authors declare no competing financial interests.

**Authors** 

**K. W. Hipps** – Department of Chemistry and Materials Science and Engineering Program, Washington State University, Pullman, Washington 99163-4630, United States; orcid.org/0000-0002-5944-5114.

**Ursula Mazur** – Department of Chemistry and Materials Science and Engineering Program, Washington State University, Pullman, Washington 99163-4630, United States; orcid.org/0000-0002-3471-4883

**Supporting Information**. A power point detailing the derivation of the adhesion energy and the desorption energy from a metal surface into solution. A pdf file containing a number of

computed structures and energies, derivation of needed thermodynamic and statistical quantities, and CONCAR files for selected optimized structure.

## **ACKNOWLEDGMENT**

This work is supported by the US National Science Foundation in the form of grant CHE1807225 and CHE-2306316. We thank Charlie Campbell (University of Washington) for several insightful conversations.

#### REFERENCES

<sup>1</sup> Kumar, S.; Choudhuri, I.; Pathak, B. An atomically thin ferromagnetic half-metallic pyrazine-fused Mn-porphyrin sheet: A slow spin relaxation system. *J. Mater. Chem. C* **2016**, *4*, 9069–9077.

- <sup>3</sup> Posligua, V.; Aziz, A.; Haver, R.; Peeks, M.D.; Anderson, H.L.; **Grau-Crespo, R**. Band Structures of Periodic Porphyrin Nanostructures. *J. Phys. Chem. C* **2018**, *122*, 23790–23798.
- <sup>4</sup> Aziz, A.; Ruiz-Salvador, A.; HernÃ; ndez, N.C.; Calero, S.; Hamad, S.; **Grau-Crespo, R**. Porphyrin-based metal-organic frameworks for solar fuel synthesis photocatalysis: Band gap tuning via iron substitutions. *J. Mater. Chem. A* **2017**, *5*, 11894–11904
- <sup>5</sup> Krasnov, P.O.; Kuzubov, A.A.; Kholtobina, A.S.; Kovaleva, E.; Kuzubova, M.V. Optical charge transfer transitions in supramolecular fullerene and porphyrin compounds. *J. Struct. Chem.* **2016**, *57*, 642–648.
- <sup>6</sup> Tian, X.; Lin, C.; Zhong, Z.; Li, X.; Xu, X.; Liu, J.; Kang, L.; Chai, G.; Yao, J. E ect of Axial Coordination of Iron Porphyrin on Their Nanostructures and Photocatalytic Performance. *Cryst. Growth Des.* **2019**, *19*, 3279–3287.

<sup>&</sup>lt;sup>2</sup> Ghosh, D.; Parida, P.; Pati, S.K. Spin-state switching of manganese porphyrin by conformational modification. *J. Phys. Chem. C* **2016**, *120*, 3625–3634.

- <sup>7</sup> Adinehnia, M.; Borders, B.; Ruf, M.; Chilukuri, B.; Hipps, K.W.; Mazur, U. Comprehensive structure-function correlation of photoactive ionic π-conjugated supermolecular assemblies: an experimental and computational study. *J. Mater. Chem. C* **2016**, *4*, 10223-10239.
- <sup>8</sup> Nandi, G.; Chilukuri, B.; Hipps, K.W.; Mazur, U. Surface directed reversible imidazole ligation to nickel (II) octaethylporphyrin at the solution/solid interface: A single molecule level study. *Phys. Chem. Chem. Phys.* 2016, 18, 20819–20829.
- <sup>9</sup> Bao, D.; Zhang, Y.; Du, S.; Pantelides, S.; Gao, H. Barrierless On-Surface Metal Incorporation in Phthalocyanine-Based Molecules. *J. Phys. Chem. C* **2018**, *122*, 6678–6683.
- <sup>10</sup> Porphyrin Reactions on Surfaces Barrierless On-Surface Metal Incorporation in Phthalocyanine-Based Molecules. Bao, D.; Zhang, Y.; Du, S.; Pantelides, S.; Gao, H. J.; *J. Phys. Chem. C* **2018**, *122*, 6678–6683.
- Hieringer, W.; Flechtner, K.; Kretschmann, A.; Seufert, K.; Auwärter, W.; Barth, J.V.; Görling, A.; Steinrück, H.; Gottfried, J.M. The surface trans effect: Influence of axial ligands on the surface chemical bonds of adsorbed metalloporphyrins. *J. Am. Chem. Soc.* 2011, 133, 6206–6222.
- <sup>12</sup> Janet, J.P.; Zhao, Q.; Ioannidis, E.I.; Kulik, H.J. Density functional theory for modelling large molecular adsorbate–surface interactions: A mini-review and worked example. *Mol. Simul.* 2017, 43, 327–345.
- Wäckerlin, C.; Tarafder, K.; Siewert, D.; Girovsky, J.; Hählen, T.; Iacovita, C.; Kleibert, A.; Nolting, F.; Jung, T.A.; Oppeneer, P.M.; et al. On-surface coordination chemistry of planar molecular spin systems: Novel magnetochemical effects induced by axial ligands. *Chem. Sci.* 2012, 3, 3154–3160.
- B. Chilukuri, R. N. McDougald Jr., M. M. Ghimire, V. N. Nesterov, U. Mazur, M. A. Omary and K.
   W. Hipps, *J. Phys. Chem. C*, 2015, *119*, 24844–24858.

- <sup>15</sup> Zotti, L.A.; Teobaldi, G.; Hofer, W.A.; Auwärter, W.; Weber-Bargioni, A.; Barth, J.V. Ab-initio calculations and STM observations on tetrapyridyl and Fe(II)-tetrapyridyl-porphyrin molecules on Ag (1 1 1). Surf. Sci. 2007, 601, 2409–2414.
- <sup>16</sup> Reimers, J.R.; Panduwinata, D.; Visser, J.; Chin, Y.; Tang, C.; Goerigk, L.; Ford, M.; Baker, M.; Sum, T.; Coenen, J.; et al. From Chaos to Order: Chain-Length Dependence of the Free Energy of Formation of Meso-tetraalkylporphyrin Self-Assembled Monolayer Polymorphs. *J. Phys. Chem. C* 2016, *120*, 1739–1748.
- De Marchi, F.; Galeotti, G.; Simenas, M.; Ji, P.; Chi, L.; Tornau, L.; Pezzella, A.; MacLeod, L.; Ebrahimi, M.; Rosei, F. Self-assembly of 5,6-dihydroxyindole-2-carboxylic acid: polymorphism of a eumelanin building block on Au(111). *Nanoscale* 2019, 11, 5422-5428.
- <sup>18</sup> Janet, J.P.; Zhao, Q.; Ioannidis, E.I.; Kulik, H.J. Density functional theory for modelling large molecular adsorbate–surface interactions: A mini-review and worked example. *Mol. Simul.* 2017, 43, 327–345.
- El Garah, M.; Dianat, A.; Cadeddu, A.; Gutierrez, R.; Cecchini, M.; Cook, T.; Ciesielski, A.; Stang, P. J.; Cuniberti, G.; Samorì, P. Atomically Precise Prediction of 2D Self-Assembly of Weakly Bonded Nanostructures: STM Insight into Concentration-dependent Architectures. Small 2016, 12, 343–350
- <sup>20</sup> Jeindl, A.; Hormann, L.; Hofmann, O. T. How much does surface polymorphism influence the work function of organic/metal interfaces? Applied Surface Science 575 (2022) 151687, 6 pp.
- <sup>21</sup> Shayeganfar, F.; Rochefort, A. Electronic Properties of Self-Assembled Trimesic Acid Monolayer on Graphene. *Langmuir* **2014**, *30*, 9707–9716.
- <sup>22</sup> Jahanbekam, A.; Chilukuri, B.; Mazur, U.; Hipps, K.W. Kinetically Trapped Two-Component Self-Assembled Adlayer. J. Phys. Chem. C 2015, 119, 25364–25376.

- <sup>23</sup> Li, W.; Jin, J.; Leng, X.; Lu, Y.; Liu, X.; Wang, L.; A size, shape and concentration controlled self-assembling structure with host–guest recognition at the liquid–solid interface studied by STM.

  Nanoscale, **2016**, *8*, 11962.
- <sup>24</sup> Li, W.; Jin, J.; Leng, X.; Lu, Y.; Liu, X.; Wang, L.; Modulation of Coordinate Bonds in Hydrogen-Bonded Trimesic Acid Molecular Networks on Highly Ordered Pyrolytic Graphite Surface. *J. Phys. Chem. C* 2016, *120*, 12605–12610.
- Gurdumov, K.; Mazur, U.; Hipps, K. W. Self-Assembly Dynamics and Stability through Concentration Control at the Solution/HOPG Interface. *J. Phys. Chem. C* **2022**, *126*, 12916–12927.
- <sup>26</sup> Gurdumov, K.; Mazur, U.; Hipps, K.W. Influences on the Dynamics and Stability of Self-Assembly: Solvent, Substrate, and Concentration. *J. Phys. Chem. C* **2022**, *126*, 19904-19915.
- Nangia, A. Pseudopolymorph: Retain This Widely Accepted Term. *Crystal Growth & Design*,
  2006, 6, 1.
- <sup>28</sup> Singh, N.; Campbell, C. T. A Simple Bond-Additivity Model Explains Large Decreases in Heats of Adsorption in Solvents Versus Gas Phase: A Case Study with Phenol on Pt(111) in Water. ACS Catal. 2019, 9, 8116–8127.
- <sup>29</sup> Rumptz, J.; Campbell, C.T. Adhesion Energies of Liquid Hydrocarbon Solvents onto Pt(111), MgO(100), Graphene, and TiO2(110) from Temperature- Programmed Desorption Energies. *J. Phys. Chem. C* 2021, *125*, 27931-27937.
- <sup>30</sup> Kresse, G.; Furthmüller, J. Efficiency of Ab-Initio Total Energy Calculations for Metals and Semiconductors Using a Plane-Wave Basis Set. *Comput. Mater. Sci.* **1996**, *6*, 15 50.
- Kresse, G.; Hafner, J. Ab Initito Molecular Dynamics for Liquid Metals. *Phys. Rev. B* 1993, 47, 558
   561.

- Gaussian 16, Revision C.01: Frisch, M. J.; Trucks, G. W.; Schlegel, H. B.; Scuseria, G. E.; Robb,
   M. A.; Cheeseman, J. R.; Scalmani, G.; Barone, V.; Petersson, G. A.; Nakatsuji, H.; et al.
   Gaussian, Inc., Wallingford CT, 2016
- <sup>33</sup> Kresse, G.; Joubert, D. From Ultrasoft Pseudopotentials to the Projector Augmented-Wave Method. *Phys. Rev. B* **1999**, *59*, 1758.
- <sup>34</sup> Blöchl, P. E. Projector Augmented-Wave Method. *Phys. Rev. B* **1994**, *50*, 17953.
- <sup>35</sup> Klimeš, J.; Bowler, D. R.; Michaelides, A. Van der Waals Density Functionals Applied to Solids. *Phys. Rev. B* **2011**, *83*, 195131.
- <sup>36</sup> Becke, A. D. Density-Functional Exchange-Energy Approximation with Correct Asymptotic Behavior. *Phys. Rev. A* **1988**, *38*, 3098.
- Peng, H.; Yang, Z.; Perdew, J. P.; Sun, J. Versatile van der Waals Density Functional Based on a Meta-Generalized Gradient Approximation. *Phys. Rev. X* **2016**, *6*, 041005. 14 pages.
- <sup>38</sup> Perdew, J. P.; Burke, K.; Ernzerhof, M. Generalized Gradient Approximation Made Simple. *Phys. Rev. Lett.* **1996**, 77 (18), 3865. Perdew, J. P.; Burke, K.; Ernzerhof, M. Generalized Gradient Approximation Made Simple. *Phys. Rev. Lett.* **1996**, 77, 3865.
- Octaethylporphyrin Monolayer on Au(111) and HOPG(0001) Substrates: A Comparative First Principles Study. Phys. Chem. Chem. Phys. 2014, 16, 14096 14107.
- <sup>40</sup> Zhang, Y.; Lee, D.; Hipps, K.W. Characterizing the CH3SSCH3-Au(111) System From Single Molecules To Full Surface Coverage: A Scanning Tunneling Microscopy Study. *J. Phys. Chem. C* 2021, *125*, 21988-21996.

- <sup>41</sup> Borders, B.; Adinehnia, M.; Chilukuri, B.; Ruf, M.; Hipps, K. W.; Mazur, U. Tuning the Optoelectronic Characteristics of Ionic Organic Crystalline Assemblies. *J. Mater. Chem. C* 2018, 6, 4041 4056.
- <sup>42</sup> Zhang, Y. C.; Chilukuri, B.; Hanson, T. B.; Heiden, Z. M.; Lee, D. Y. Connecting Solution-Phase to Single-Molecule Properties of Ni(Salophen). *J. Phys. Chem. Lett.* **2019**, *10*, 3525 3530.
  - 43 G. Mills, H. Jonsson and G. K. Schenter, Surface Science, 324, 305 (1995); H. Jonsson, G.
     Mills and K. W. Jacobsen, 'Nudged Elastic Band Method for Finding Minimum Energy
     Paths of Transitions', in 'Classical and Quantum Dynamics in Condensed Phase
     Simulations', ed. B. J. Berne, G. Ciccotti and D. F. Coker (World Scientific, 1998)
  - <sup>44</sup> Hill, T. L. *An introduction to Statistical Thermodynamics*, Chapter 11, Dover Publications, 2986, New York, **1986**.
  - <sup>45</sup> Tahara, K.; Balandina, T.; Furukawa, S.; De Feyter, S.; Tobe, Y. Molecular pentagonal tiling: self-assemblies of pentagonal-shaped macrocycles at liquid/solid interfaces.
    CrystEngComm, 2011, 13, 5551-5558.
  - <sup>46</sup> Genesh, N.; Cui, D.; Dettmann, D.; MacLean, O.; Johal, T.; Lunchev, A.; Grmsdale, A.; Rosei,
     F. Selective Self-Assembly and Modification of Herringbone Reconstructions at a Solid-Liquid Interface of Au(111). *J. Phys. Chem. Lett.* 2023, *14*, 3057-3062.
  - <sup>47</sup> Haro, D.; Matsushita, L.; Kong, M.; Rodriguez-Reyes, C. Temperature-Programmed Reactions of Aromatic Compounds on Au(111) and on a Model Gold Catalyst. *J. Phys. Chem. C*, **2022**, *126*, 20364-20374.

43

- <sup>48</sup> Mammen, M.; Shakhnovich,, E.I.; Deutch, J. M.; Whitesides, G. M. Estimating the Entropic Cost of Self-Assembly of Multiparticle Hydrogen-Bonded Aggregates Based on the Cyanuric Acid-Melamine Lattice. *J. Org. Chem.* **1998**, *63*, 3821-3830.
- <sup>49</sup> Green, J.; Harrison, D.; Kynaston, W. Vibrational spectra of benzene derivatives-XII. *Spectrochim. Acta*, **1971**, *27A*, 807-815.
- <sup>50</sup> Yie, Y.; Boggs, J.E.; The Computed Force Constants and Vibrational Spectra of Toluene. *J. Comput. Chem.*, **1986**, *7*, 158-164.
- <sup>51</sup> Fuson, N.; Garrigou-Lagrange, C.; Josien, M. Spectre infrarouge et attribution des vibrations des toluènes C<sub>6</sub>H<sub>5</sub>CH<sub>3</sub>, C<sub>6</sub>H<sub>5</sub>CD<sub>3</sub> et C<sub>6</sub>D<sub>5</sub>CD<sub>3</sub>. *Spectrochim. Acta*, **1960**, *16*, 106-127.
- <sup>52</sup>Sprowl, L.; Campbell, C.T.; Arnadottir, L. Hindered Translator and Hindered Rotor Models for Adsorbates: Partition Functions and Entropies. *J. Phys. Chem. C* **2016**, *120*, 9719-9731.
- <sup>53</sup> McClurg, R.; Flagan, R. The hindered rotor density-of-states interpolation function. *J. Chem. Phys.* **1997**, *106*, 6675-6680.
- <sup>54</sup> Campbell, C.T.; Mao, Z. Analysis and prediction of reaction kinetics using the degree of rate control. *J. Catal.* **2021**, *404*, 647-660.
- <sup>55</sup> Eyring, H. The Theory of Absolute Reaction Rates, *Trans. Fraday Soc.* **1938**, *34*, 41-48.
- <sup>56</sup> Campbell, C.T.; Sprowl, Arnadottir, L. Equilibrium Constants and Rate Constants for Adsorbates: Two-Dimensional (2D) Ideal Gas, 2D Ideal Lattice Gas, and Ideal Hindered Translator Models. J. Phys. Chem. C 2016, 120, 10283-10297.
- <sup>57</sup> Knopf, D.; Ammann, M. Technical note: Adsorption and desorption equilibria from statistical thermodynamics and rates from transition state theory. *Atmos. Chem. Phys.* **2021**, *21*, 15725-15753.

- <sup>58</sup> Thrower, J.; Friis, E.; Skov, A.; Nilsson, L.; Anderson, M.; Ferrighi, B.; Jorgensen, B.; Baouche, S.; Balog, R.; Hammer, B.; et al. Interaction between Coronene and Graphite from Temperature-Programmed Desorption and DFT-vdW Calculations: Importance of Entropic Effects and Insights into Graphite Interlayer Binding. *J. Phys. Chem. C.* 2013, 117, 13520-13529.
- <sup>59</sup> Kórósi, G.; Kováts, E. Density and Surface Tension of 83 Organic Liquid. *J. Chem. Eng. Data* 1981, 26, 323-332
- <sup>60</sup> Akinola, J.; Campbell, C. T.; Singh, N. Effects of Solvents on Adsorption Energies: A General Bond-Additivity Model. J. Phys. Chem. C 2021, 125, 24371-24380.
- <sup>61</sup> Bhattari, A.; Mazur, U.; Hipps, K. W. A Single Molecule Level Study of the Temperature-Dependent Kinetics for the Formation of Metal Porphyrin Monolayers on Au(111) from Solution. *J. Am. Chem. Soc.* **2014**, *136*, 2142–2148
- <sup>62</sup> Jung, L.; Campbell, C. Sticking Probabilities in Adsorption of Alkanethiols from Liquid Ethanol Solution onto Gold. *J. Phys. Chem. B* 2000,104,11168-11178
- <sup>63</sup> Perlovich, G.; Golubchikov, O.; Lueva, M. J. Thermodynamics of porphyrin sublimation. Porphyrins Phthalocyanines 2000, 4, 699–706.
- <sup>64</sup> Foresman, J.B.; Frisch, A. *Exploring Chemistry with Electronic Structure Methods:* 3<sup>rd</sup> Ed. Chapter 5, Gaussian Inc. **2015**.

# **TOC GRAPHIC**

